Effect of Defective NPC Three Level Inverter on Nonlinear Command of Induction Motor

Mendaz Kheira[1], Benhadda Yamina[2], Bounoua Houria[3]

Abstract: Speed Induction Motor (IM) control is an area of research that has been in evidence for some time now. In this paper, a nonlinear controller is presented for the induction motor drives. The nonlinear controller is designed based on an input-output feedback linearization control technique. The input-output feedback linearization control decouples the flux from the speed control and makes the synthesis of linear controllers possible. This article presented input-output linearization control of the induction motor associated with NPC three level inverter defective, the inverter faults are usually caused by operating faults in the switch elements. Switching defects occur in rectifier diodes, the capacitor and inverter IGBT switches. The inverter switches defected reduce the performance of the motor, in our study. We applied the input-output linearization control to test their robustness and performance for detection of fault influence on the physical parameters of the motor, for this purpose, we applied two faults, we started by creating a fault in two switches K_1 and K_7 which are in the first and second arm of the inverter. Then we created a fault in the three switches K_1, K_7 and K_{10} which are in the three arms of the inverter. The simulation results are done by the use of Matlab/Simulink that show the detection, fault effect on input-output linearization control of the different induction motor responses.

Keywords: Induction motor, Input Output linearization control, Switch fault Inverter, Performance, Robustness.

1 Introduction

Today, alternating current machines can replace the direct current machine in most variable speed applications. In particular, an induction motor is considered the preferred actuator constant speed applications. It offers some advantages compared to the DC motor, such as its ease of manufacture and maintenance, without a brush-collector device, its weight, and low inertia, with

---

[1]Electrical engineering department, IRECOM laboratory, Belhadj Bouchaib University, Algeria;
 E-mail: kheiramendez@gmail.com
[2]Electrical engineering department, LEP laboratory, Mohamed Boudiaf University Oran, Algeria;
 Email: Benhadda_yamina@yahoo.fr
[3]Electrical Engineering Department, IRECOM laboratory, Djillali Liabes University School of Engineering Science, Sidi Bel Abbes, Algeria; E-mail: hsmmach@yahoo.fr

an excellent performance. It is also appreciated for its reliability and robustness. However, the simplicity of its mechanical structure is accompanied by a high complexity in the mathematical model (multi-variable and non-linear).

Due to the significant influence of nonlinearities on induction motor system dynamics, linear control techniques are quite good, and they may not meet the system specifications, mainly in the case of variable speed applications. Among these nonlinear techniques that ensure high performance and global decoupling between the outputs to control whatever the path profile imposed for the machine, one can mention the input-output linearization technique.

This method implements the differential geometry theory to transform a nonlinear system into a linear one by using a state feedback linearizing method that ensures input-output decoupling [1, 2].

The major merit of this technique is that one can find a global feedback law to linearize and decouple multi-input multi-output (MIMO) nonlinear system, where regular linear design methods can be applied.
The input-output linearization control is an analytical design approach which aims to reduce the original nonlinear problem to a simpler linear control problem. The nonlinear control system is designed using a two-step procedure.

Firstly, a nonlinear process model is used to synthesize a nonlinear state feedback controller that linearized the map between a new manipulated input and the controlled output. In the second step, a linear pole placement controller is designed for the feedback linearized system [4].

Induction motor drives using the input-output feedback linearization technique in order to decompose the motor model into two separate subsystems, rotor speed and rotor flux amplitude [6].

The power electronics part is considered as the weakest component in the drive system, and about 38% of the induction motor faults are due to switching faults. In this section the causes and effects of various switching faults in the induction motor performance are described. Switching faults may occur due to many reasons, which include electrical stress due to stored charge carriers, maximum reverse current, faulty base drive system, manufacturing defects, ageing of the capacitor, loose connections, abnormal transients, etc. It can result in reduced performance of the motor, increase in temperature resulting in an increase in stator current or may even result in the shutdown of the motor [7].

Multilevel inverter offers interesting advantages such as possibility of operation in medium, high voltage and high power applications, providing a better voltage waveform with low total harmonic distortion for electric machine applications.

However, the number of switches needed in the topology increases with the number of levels and, although the switches may be highly reliable, a system's

fault probability will become increasing. An unbalanced voltage is generated when a fault occurs, which can produce permanent damage to the load or complete system failure [10, 11].

Harmonic currents/voltages are created by nonlinear devices which induced in power systems and eventually flow back to the source; there are few methods to reduce the harmonics such as filter technique. Harmonic filters are broadly classified into passive and active filters. Passive filters, as the name implies, it is constructed with passive components such as resistors, inductors, and capacitors. In filter technique, there are many designs based on inductors and capacitors to reduce the harmonics, such as LCL. Filter technique is adopted to reduce the harmonics and THD in three-level NPC inverter [16, 17].

This article discus about input-output linearization control with application of switch fault for three-level NPC inverter.

Result simulation using Matlab shows the effect of these defects on physical parameters of the induction motor and show the performance and robustness given by input output linearization control. After keywords, the first section is usually Introduction, although some other subtitles can be used.

2   Mathematical Modeling of Induction Motor

The mathematical model of the induction motor is used for analyzing the dynamic behaviour of the motor. The change in the dynamic behavior of the motor affects the motor parameters such as speed, torque, resistance, flux analyzing the change in performance of the induction motor. A dynamic model of the induction motor is derived by transforming the three-phase quantities into two phases axes quantities (Clark transforms). Mathematical equation of the induction motor is given below ($\alpha\beta$ rotating) wish rewritten in rotation reference frame [21]:

$$\frac{d\Omega}{dt} = \frac{n_p L_m}{J L_r} \left(\varphi_{r\alpha} I_{s\beta} - \varphi_{r\beta} I_{s\alpha} \right) - \frac{1}{J} T_l - \frac{1}{J} f\Omega, \qquad (1)$$

$$\frac{d I_{s\alpha}}{dt} = -\lambda I_{s\alpha} + \frac{K}{\tau_r} \varphi_{r\alpha} + \Omega K \varphi_{r\beta} + \frac{1}{\sigma L_s} U_{s\alpha}, \qquad (2)$$

$$\frac{d I_{s\beta}}{dt} = -\lambda I_{s\beta} - \Omega K \varphi_{r\alpha} - \frac{K}{\tau_r} \varphi_{r\beta} + \frac{1}{\sigma L_s} U_{s\beta}, \qquad (3)$$

$$\frac{d\varphi_{r\alpha}}{dt} = \frac{L_m}{\tau_r} I_{s\alpha} - \frac{1}{\tau_r} \varphi_{r\alpha} - \Omega \varphi_{r\beta}, \qquad (4)$$

$$\frac{\mathrm{d}\varphi_{r\beta}}{\mathrm{d}t} = \frac{L_m}{\tau_r} I_{s\beta} - \Omega\varphi_{r\alpha} - \frac{1}{\tau_r}\varphi_{r\beta}, \tag{5}$$

where $\tau_r = \dfrac{L_r}{R_r}$, $\sigma = 1 - \dfrac{L_m^2}{L_s L_r}$, $T_e = \dfrac{n_p L_m}{JL_r}\left(\varphi_{r\alpha}I_{s\beta} - \varphi_{r\beta}I_{s\alpha}\right)$, $\lambda = \dfrac{L_m^2 R_r}{L_r^2 \sigma L_s} + \dfrac{R_s}{\sigma L_s}$,

$K = \dfrac{L_m}{L_r \sigma L_s}$, σ – scattering coefficient Blondel, n_p – Number of pole pairs, L_m –

mutual inductance, τ_r – rotor time constant, L_s, L_r – stator and rotor inductance, J – inertia, f – friction of the rotor, $\varphi_{r\alpha}$, $\varphi_{r\beta}$ – arm of the flux generated by the rotor on the axes $\alpha\beta$, T_e – electromagnetic torque, $I_{s\alpha}$, $I_{s\beta}$ – stator current on the axes $\alpha\beta$ and Ω – speed.

3 Input Output Linearization Control

The objective of state feedback-exact linearization is to create a linear differential relation between the output y_1, y_2 and an internal defined input V_1, V_2 an important property of a nonlinear system is its relative degree. The output needs to be differentiated for r times until it is directly related to the input. The number r is called the relative degree of the system [3 – 5].

The approach in obtaining the exact linearization of the multi input multi output systems is to differentiate the output y_j until the input reveals, is given by:

$$\frac{\mathrm{d}y_j}{\mathrm{d}t} = L_f h_j + \sum_{i=1}^{m} L_{gi} h_j(x) U_i, \tag{6}$$

where $L_f h_j$ represents derivatives of the smooth scalar function of $h_j(x)$ with respect to $f(x)$, which is defined as:

$$L_f h_j = \frac{\mathrm{d}h_j(x)}{\mathrm{d}x} f(x). \tag{7}$$

Similarly, in the case of another vector field $L_{gi} h_j(x)$ given by:

$$L_{gi} h_j(x) = \frac{\mathrm{d}h_j(x)}{\mathrm{d}x} g_i(x). \tag{8}$$

Assuming that r_j is the smallest integer for which at least one of the inputs appears in $y_j^{(r_j)}$, which is defined as:

$$y_j^{(r_j)} = L_f^{r_j} h_j + \sum_{i=1}^{m} L_g^{r_j} h_j(x) U_i, \tag{9}$$

with $L_g^{r_j} h_j(x) \neq 0$ for all least one i. If we perform the above procedure for each input y_j, we can obtain a total of m equations in the above form, which can be written completely as:

$$\begin{bmatrix} y_j^n \\ . \\ . \\ . \\ y_j^{r_m} \end{bmatrix} = \begin{bmatrix} L_f^n h_1(x) \\ . \\ . \\ . \\ L_f^{r_m} h_j(x) \end{bmatrix} + D(x) \begin{bmatrix} U_1 \\ . \\ . \\ . \\ U_m \end{bmatrix}, \tag{10}$$

where the $m \times m$ matrix $D(x)$ is defined as:

$$D(x) = \begin{bmatrix} L_{g1}^{n-1} h_j & . & . & . & L_{gm}^{n-1} h_j \\ . & & & & \\ . & & . & . & . \\ . & & . & . & . \\ . & & & & \\ L_{g1}^{r_{m-1}} h_j & . & . & . & L_{gm}^{r_{m-1}} h_j \end{bmatrix}, \tag{11}$$

The matrix $D(x)$ is called the decoupling matrix of the MIMO system. If $D(x)$ is nonsingular, then the input transformation can be obtained as:

$$\begin{bmatrix} U_1 \\ . \\ . \\ . \\ U_m \end{bmatrix} = D^{-1}(x) \left(\begin{bmatrix} y_j^n \\ . \\ . \\ . \\ y_j^{r_m} \end{bmatrix} - \begin{bmatrix} L_f^n h_1(x) \\ . \\ . \\ . \\ L_f^{r_m} h_j(x) \end{bmatrix} \right), \tag{12}$$

Substituting (11) into (12) results in a linear differential relation between the output y and the new input V:

$$\begin{bmatrix} y_j^n \\ . \\ . \\ . \\ y_j^{r_m} \end{bmatrix} = \begin{bmatrix} V_1 \\ . \\ . \\ . \\ V_m \end{bmatrix}. \tag{13}$$

Note that the above input-output relation is decoupled, in addition to being linear.

Since the new input *V*, only affects the output *y*, (12) is called a decoupling control law, and the invertible matrix $D(x)$ is called the decoupling matrix of the system. The system (9) is then said to have a relative degree $(r_j, \ldots, r_m)$ at x_0 and the scalar $r = r_j + \cdots + r_m$ is called the total relative degree of the system at x_0.

4   Input Output Linearization Control of Induction Motor

The choice of outputs is according to the objectives of control. The rotor speed is chosen as the first output while the second output selected is the square of the rotor flux, so as for tracking the purposed control trajectory [4, 5],

$$y(x) = \begin{bmatrix} h_1(x) \\ h_2(x) \end{bmatrix} = \begin{bmatrix} \Omega \\ \varphi_{\alpha r}^2 + \varphi_{\beta r}^2 \end{bmatrix}. \tag{14}$$

The time derivative of the system output $h_1(x)$ can be expressed as:

$$y_1 = h_1(x) = \Omega, \tag{15}$$

$$\frac{d y_1}{d t} = \frac{d h_1(x)}{d t} = \frac{d \Omega}{d t}, \tag{16}$$

$$\frac{d y_1}{d t} = L_f h_1(x) + L_{g1} h_1(x) \; U_{s\alpha} + L_{g2} h_1(x) U_{s\beta}, \tag{17}$$

$$\frac{d y_1}{d t} = \frac{n_p L_m}{J L_r} \left(\varphi_{r\alpha} I_{s\beta} - \varphi_{r\beta} I_{s\alpha} \right) - \frac{1}{J} T_l - \frac{1}{J} f \Omega, \tag{18}$$

where T_l is load torque.

The time derivative of the system output $h_2(x)$ can be expressed as:

$$y_2 = h_2(x) = \varphi_r^2, \tag{19}$$

$$\frac{d y_2}{d t} = \frac{d h_2(x)}{d t} = \frac{d \varphi_r^2}{d t}, \tag{20}$$

$$\frac{d y_2}{d t} = L_f h_2(x) + L_{g1} h_2(x) U_{s\alpha} + L_{g2} h_2(x) U_{s\beta}, \tag{21}$$

$$\varphi_r^2 = \varphi_{r\alpha}^2 + \varphi_{r\beta}^2, \tag{22}$$

$$\frac{d y_2}{d t} = \frac{d \varphi_r^2}{d t} = \frac{2}{\tau_r} \left(L_m \left(\varphi_{\alpha r} I_{s\beta} + \varphi_{\beta r} I_{s\alpha} \right) - \left(\varphi_{r\alpha}^2 + \varphi_{r\beta}^2 \right) \right). \tag{23}$$

Note that for a controllable system, we always have $r \leq n$, with n as the system order.

The total relative degree is defined as the sum of all the relative degrees, it must be less than or equal to the system order $[1-3]$.

In the case of the induction motor system, it is easy to verify that the control can't appear for the first time in the first derivative of the outputs y_1 and y_2 so we derivative the outputs $d\,y_1/dt$ and $d\,y_2/dt$ for the second time, that presented in the following $[4]$:

$$\frac{d^2\, y_1}{dt^2} = \frac{d^2\, h_1(x)}{dt^2} = \frac{d^2\, \Omega}{dt^2}, \tag{24}$$

$$\frac{d^2\, y_1}{dt^2} = L_f^2 h_1(x) + L_{g1} L_f h_1(x) U_{s\alpha} + L_{g2} L_f h_1(x) U_{s\beta}, \tag{25}$$

$$\frac{d^2\, y_1}{dt^2} = -\frac{n_p L_m}{J L_r} K\Omega\left(\varphi_{r\beta}^2 + \varphi_{r\alpha}^2\right) - \left(\frac{n_p L_m}{J L_r}\left(\frac{1}{\tau_r} + \lambda\right)\right)\left(\varphi_{\alpha r} I_{s\beta} - \varphi_{r\beta} I_{s\alpha}\right) -$$
$$-\frac{n_p L_m}{J L_r}\Omega\left(\varphi_{r\beta} I_{s\beta} + \varphi_{\alpha r} I_{s\alpha}\right) - \frac{n_p L_m}{J L_r \sigma L_s}\varphi_{r\beta} U_{s\alpha} + \frac{n_p L_m}{J L_r \sigma L_s}\varphi_{\alpha r} U_{s\beta}, \tag{26}$$

$$\frac{d^2\, y_2}{dt^2} = \frac{d^2\, h_2(x)}{dt^2} = \frac{d^2\, \varphi_r^2}{dt^2}, \tag{27}$$

$$\frac{d^2\, y_2}{dt^2} = L_f^2 h_2(x) + L_{g1} L_f h_2(x) U_{s\alpha} + L_{g2} L_f h_2(x) U_{s\beta}, \tag{28}$$

$$\frac{d^2\, y_2}{dt^2} = \left(2\left(\frac{1}{\tau_r}\right)^2 (2 + k L_m)\right)\left(\varphi_{r\alpha}^2 + \varphi_{r\beta}^2\right) + \left(\frac{2 n_p L_m}{\tau_r}\right)\left(\Omega(\varphi_{\alpha r} I_{s\beta} + \varphi_{r\beta} I_{s\alpha})\right) -$$
$$-\left(\left(6\left(\frac{1}{\tau_r}\right)^2 L_m\right) + \left(\frac{2\lambda L_m}{\tau_r}\right)\right)\left(\varphi_{r\beta} I_{s\beta} + \varphi_{\alpha r} I_{s\alpha}\right) +$$
$$+\left(2\left(\frac{L_m}{\tau_r}\right)^2\right)\left(I_{s\alpha}^2 + I_{s\beta}^2\right) + \frac{2 n_p L_m^2}{J L_r \sigma L_s}\varphi_{\alpha r} U_{s\alpha} + \frac{2 n_p L_m^2}{J L_r \sigma L_s}\varphi_{r\beta} U_{s\beta}. \tag{29}$$

The degree of $h_1(x)$ and $h_2(x)$ is $r_1 = r_2 = 2$.

The global relative degree is lower than the order n of the system $r = r_1 + r_2 = 4 < n < 5$.

The matrix defines a relation between the input $(U_{s\alpha}, U_{s\beta})$ and the output (y_1, y_2) is given by the expression (30):

$$\begin{bmatrix} \dfrac{\mathrm{d}^2\,y_1}{\mathrm{d}t^2} \\[2ex] \dfrac{\mathrm{d}^2\,y_2}{\mathrm{d}t^2} \end{bmatrix} = A(x) + D(x)\begin{bmatrix} U_{\alpha s} \\[1ex] U_{s\beta} \end{bmatrix}, \tag{30}$$

$$A(x) = \begin{bmatrix} L_f^2 h_1(x) \\[1ex] L_f^2 h_2(x) \end{bmatrix}, \tag{31}$$

$$L_f^2 h_1(x) = -\frac{\left(n_p L_m\right)^2}{L_r J^2}\left(\varphi_{\alpha r}\,I_{s\beta} - \varphi_{r\beta}\,I_{s\alpha}\right) + \frac{n_p L_m\,f^2}{L_r J^3}\Omega -$$

$$-\frac{n_p L_m}{JL_r}K\Omega\left(\varphi_{r\beta}^2 + \varphi_{r\alpha}^2\right) - \left(\frac{n_p L_m}{L_r}\left(\frac{1}{\tau_r} + \lambda\right)\right)\left(\varphi_{\alpha r}\,I_{s\beta} - \varphi_{r\beta}\,I_{s\alpha}\right) - \tag{32}$$

$$-\frac{n_p L_m}{JL_r}\Omega\left(\varphi_{r\beta}I_{s\beta} + \varphi_{\alpha r}I_{s\alpha}\right),$$

$$L_f^2 h_2(x) = \left(2\left(\frac{n_p L_m}{JL_r}\right)^2\left(2 + kL_m\right)\right)\left(\varphi_{\alpha r} + \varphi_{r\beta}^2\right) + \left(\frac{2n_p^2 L_m^2}{JL_r}\right)\Omega\left(\varphi_{\alpha r}I_{s\beta} + \varphi_{r\beta}\,I_{s\alpha}\right)$$

$$-\left(\left(6\left(\frac{n_p L_m}{JL_r}\right)^2 L_m\right) + \left(\frac{2\lambda n_p L_m^2}{JL_r}\right)\right)\left(\varphi_{r\beta}I_{s\beta} + \varphi_{\alpha r}I_{s\alpha}\right) + \tag{33}$$

$$+\left(2\left(\frac{n_p L_m^2}{JL_r}\right)^2\right)\left(I_{s\alpha}^2 + I_{s\beta}^2\right),$$

$$D(x) = \begin{bmatrix} L_{g1}L_f h_1 & L_{g2}L_f h_1 \\[1ex] L_{g1}L_f h_2 & L_{g2}L_f h_2 \end{bmatrix} = \begin{bmatrix} \dfrac{n_p L_m}{JL_r \sigma L_s}\varphi_{r\beta} & \dfrac{n_p L_m}{JL_r \sigma L_s}\varphi_{\alpha r} \\[2ex] \dfrac{2n_p L_m^2}{JL_r \sigma L_s}\varphi_{\alpha r} & \dfrac{2n_p L_m^2}{JL_r \sigma L_s}\varphi_{r\beta} \end{bmatrix}. \tag{34}$$

The nonlinear feedback provide to the system a linear comportment input/output:

$$\begin{bmatrix} \dfrac{\mathrm{d}^2\,y_1}{\mathrm{d}t^2} \\[2ex] \dfrac{\mathrm{d}^2\,y_2}{\mathrm{d}t^2} \end{bmatrix} = \begin{bmatrix} V_1 \\[1ex] V_2 \end{bmatrix}, \tag{35}$$

$$\begin{bmatrix} U_{\alpha s} \\ U_{s\beta} \end{bmatrix} = \boldsymbol{D}^{-1}(x)\begin{bmatrix} V_1 - L_f^2 h_1(x) \\ V_2 - L_f^2 h_2(x) \end{bmatrix}. \tag{36}$$

5   Speed and Flux Control of Linear System

The internal outputs (V_1, V_2) are definite [9, 10]:

$$V_1 = \frac{d^2 y_1}{dt^2} = \frac{d^2 \Omega}{dt^2}, \tag{37}$$

$$V_2 = \frac{d^2 y_2}{dt^2} = \frac{d^2 \varphi_r^2}{dt^2}, \tag{38}$$

$$V_1 = \frac{d^2 e_1}{dt^2} + K_{11}\frac{de_1}{dt} + K_{12}e_1, \tag{39}$$

$$V_2 = \frac{d^2 e_2}{dt^2} + K_{21}\frac{de_2}{dt} + K_{22}e_2, \tag{40}$$

$$V_1 = \left(\frac{d^2 \Omega_{ref}}{dt^2} - \frac{d^2 \Omega_r}{dt^2}\right) + K_{11}\left(\frac{d\Omega_{ref}}{dt} - \frac{d\Omega}{dt}\right) + K_{12}\left(\Omega_{ref} - \Omega\right), \tag{41}$$

$$V_2 = \left(\frac{d^2 \varphi_{rref}^2}{dt^2} - \frac{d\varphi_r^2}{dt}\right) + K_{21}\left(\frac{d\varphi_{rref}^2}{dt} - \frac{d\varphi_r^2}{dt}\right) + K_{22}(\varphi_{rref}^2 - \varphi_r^2). \tag{42}$$

The error of the track is given by flowing equation:

$$\frac{d^2 e_1}{dt^2} + K_{11}\frac{de_1}{dt} + K_{12}e_1 = 0, \tag{43}$$

$$\frac{d^2 e_2}{dt^2} + K_{21}\frac{de_2}{dt} + K_{22}e_2 = 0, \tag{44}$$

$$e_1 = \Omega_{ref} - \Omega, \tag{45}$$

$$\frac{de_1}{dt} = \frac{d\Omega_{ref}}{dt} - \frac{d\Omega}{dt}, \tag{46}$$

$$e_2 = \varphi_{rref}^2 - \varphi_r^2, \tag{47}$$

$$\frac{de_2}{dt} = \frac{d\varphi_{rref}^2}{dt} - \frac{d\varphi_r^2}{dt}, \tag{48}$$

Therefore, (36) becomes:

$$\begin{bmatrix} U_{\alpha s} \\ U_{\beta s} \end{bmatrix} = \boldsymbol{D^{-1}}(x) \begin{bmatrix} \dfrac{\mathrm{d}^2\,\Omega_{ref}}{\mathrm{d}t^2} + K_{11}\left(\dfrac{\mathrm{d}\Omega_{ref}}{\mathrm{d}t} - \dfrac{\mathrm{d}\Omega}{\mathrm{d}t}\right) + K_{12}\left(\Omega_{ref} - \Omega\right) - L_f^2 h_1(x) \\ \dfrac{\mathrm{d}^2\,\varphi_{rref}^2}{\mathrm{d}t^2} + K_{21}\left(\dfrac{\mathrm{d}\varphi_{rref}^2}{\mathrm{d}t} - \dfrac{\mathrm{d}\varphi_r^2}{\mathrm{d}t}\right) + K_{22}(\varphi_{rref}^2 - \varphi_r^2) - L_f^2 h_2(x) \end{bmatrix}, \quad (49)$$

where the coefficients K_{11}, K_{12}, K_{21} and K_{22} are choosing to satisfy asymptotic stability and excellent tracking [1].

Derivation of the flux and speed transfer function goes as follows:

$$\frac{\mathrm{d}^2 e_1}{\mathrm{d}t^2} + K_{11}\frac{\mathrm{d}e_1}{\mathrm{d}t} + K_{12}e_1 = 0, \tag{50}$$

$$\frac{\mathrm{d}^2 e_2}{\mathrm{d}t^2} + K_{21}\frac{\mathrm{d}e_2}{\mathrm{d}t} + K_{22}e_2 = 0, \tag{51}$$

$$\left(\frac{\mathrm{d}^2 \Omega_{ref}}{\mathrm{d}t^2} - \frac{\mathrm{d}^2 \Omega_r}{\mathrm{d}t^2}\right) + K_{11}\left(\frac{\mathrm{d}\Omega_{ref}}{\mathrm{d}t} - \frac{\mathrm{d}\Omega}{\mathrm{d}t}\right) + K_{12}\left(\Omega_{ref} - \Omega\right) = 0, \tag{52}$$

$$\left(\frac{\mathrm{d}^2 \varphi_{rref}^2}{\mathrm{d}t^2} - \frac{\mathrm{d}\varphi_r^2}{\mathrm{d}t}\right) + K_{21}\left(\frac{\mathrm{d}\varphi_{rref}^2}{\mathrm{d}t} - \frac{\mathrm{d}\varphi_r^2}{\mathrm{d}t}\right) + K_{22}(\varphi_{rref}^2 - \varphi_r^2) = 0, \tag{53}$$

where:

$$\frac{\mathrm{d}^2 \Omega_{ref}}{\mathrm{d}t^2} = 0, \quad \frac{\mathrm{d}\Omega_{ref}}{\mathrm{d}t} = 0, \quad \frac{\mathrm{d}^2 \varphi_{rref}^2}{\mathrm{d}t^2} = 0, \quad \frac{\mathrm{d}\varphi_{rref}^2}{\mathrm{d}t} = 0,$$

$$\frac{\mathrm{d}^2\Omega_r}{\mathrm{d}t^2} + K_{11}\frac{\mathrm{d}\Omega_r}{\mathrm{d}t} + K_{12}\Omega_r = K_{12}\Omega_{rref}, \tag{54}$$

$$\frac{\mathrm{d}^2\varphi_r^2}{\mathrm{d}t^2} + K_{21}\frac{\mathrm{d}\varphi_r^2}{\mathrm{d}t} + K_{22}\varphi_r^2 = K_{22}\varphi_{rref}^2. \tag{55}$$

From (54) and (55) the speed and flux transfer functions are given by the following equations:

$$\frac{\Omega_r(s)}{\Omega_{rref}(s)} = \frac{K_{12}}{K_{12} + K_{11}s + s^2}, \tag{56}$$

$$\frac{\varphi_r^2(s)}{\varphi_{rref}^2(s)} = \frac{K_{22}}{K_{22} + K_{21}s + s^2}. \tag{57}$$

In closed loops, the flux and speed transfer functions have second-order dynamics. By identifying them to the canonical form:

$$\begin{cases} K_{11} = 2\varepsilon\omega_{n1} \\ K_{12} = \omega_{n1}^2 \end{cases} \quad \text{and} \quad \begin{cases} K_{21} = 2\varepsilon\omega_{n2} \\ K_{22} = \omega_{n2}^2 \end{cases},$$

wish:

$$\omega_{n1} = 30 \left[\frac{\text{rad}}{s} \right], \quad \varepsilon = 1, \quad \omega_{n2} = 60 \left[\frac{\text{rad}}{s} \right],$$

$$\begin{cases} K_{11} = 60, \\ K_{12} = 900, \end{cases} \quad \begin{cases} K_{21} = 120, \\ K_{22} = 3600. \end{cases}$$

The Fig. 1 shows the command of induction motor using input-output linearization control associated with three-level NPC inverter. Input-output linearization control transforms a nonlinear system dynamic into a linear system, so that linear techniques can be applied.
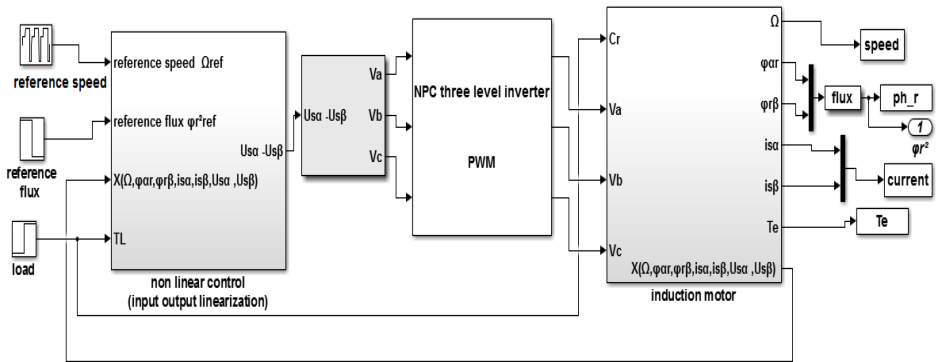
Fig. 1 – *Input output linearization control of induction motor associated with NPC three levels inverter.*

There are two control inputs for the given system $(U_{s\alpha}, U_{s\beta})$; we should have two outputs for input-output decoupling. One control input is used to regulate the input speed Ω and the other is for the flux φ_r^2 .

The Fig. 2 shows input-output linearization control of induction motor.

The central goal of input-output linearization is to design a nonlinear control law, as assumed that the inner loop control is, in the most suitable case, precisely linearized the nonlinear system after appropriate state space modification of coordinates. The developer can then build an outer-loop-control in the new coordinates to obtain a linear relation between the output and the internal input and to satisfy the traditional control design specifications such as tracking, disturbance rejection, as shown in Fig. 2.
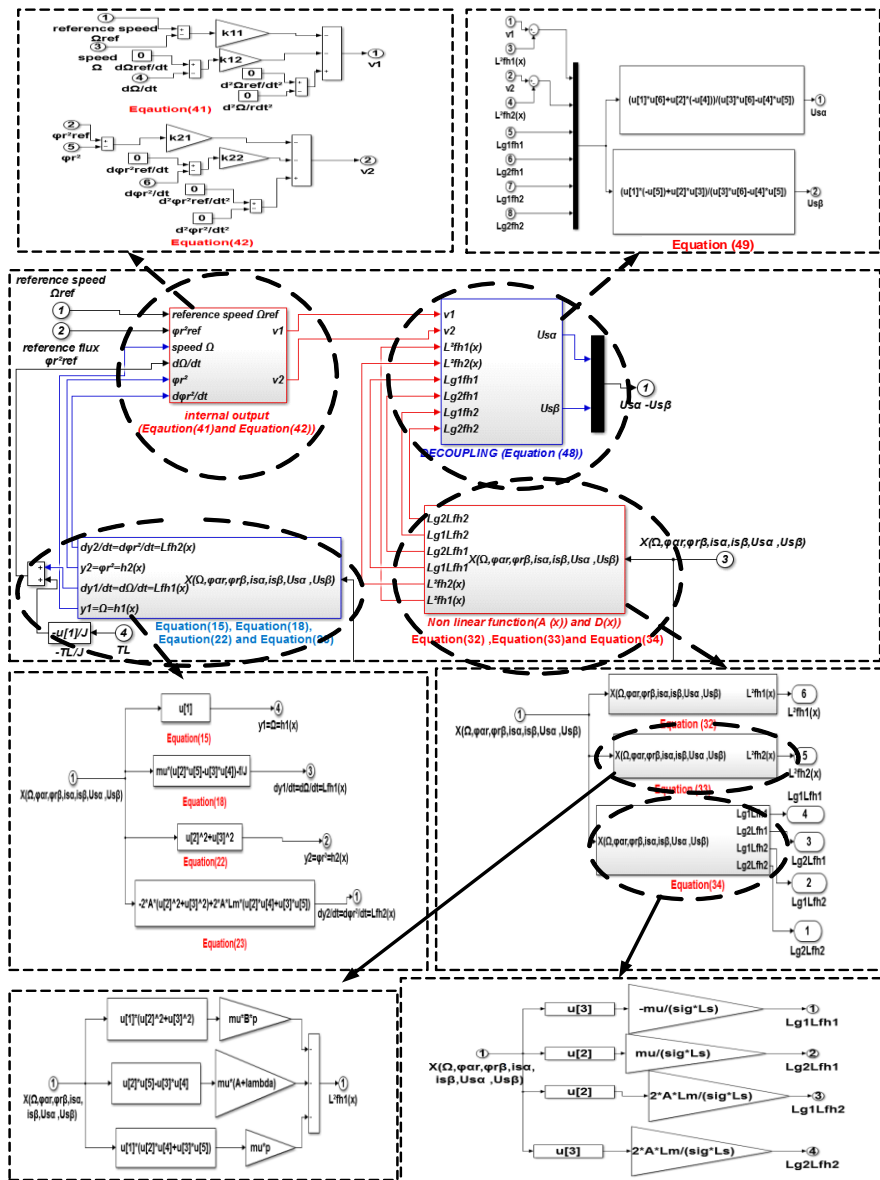
Fig. 2 − *Input output linearization control of induction machine model with appropriate subblocks in Simulink.*

As can be seen in Fig. 2, the new inputs (V_1, V_2) pass through the linearizing expressions which, at the same time, serve to decouple the control variables. The

original system will continue receiving the inputs $U_{\alpha s}$, $U_{\beta s}$ which are handled by the linearizing block in order to comply with the linearity between inputs V_1, V_2 and outputs y_1, y_2.

$$u(1) = \Omega, \quad u(2) = \varphi_{\alpha r}, \quad u(3) = \varphi_{r\beta}, \quad u(4) = I_{s\alpha}, \quad u(5) = I_{s\beta}, \quad A = 1/\tau_r, \quad p = n_p,$$

$$mu = \frac{n_p L_m}{JL_r}, \quad B = K = \frac{L_m}{L_r \sigma L_s}, \quad lambda = \lambda = \frac{L_m^2 R_r}{L_r^2 \sigma L_s} + \frac{R_s}{\sigma L_s}, \quad \sigma = \text{sig}.$$

6   Three- Level NPC Inverter Structure

The three-phase three-level NPC converter is shown in Fig. 4, the three phases have a common DC bus, divided by two capacitors into three levels. The voltage across each capacitor is $V_{dc}/2$; and the voltage stress across each switching device is limited to $V_{dc}/2$ through the clamping diodes. A three-level NPC inverter is able to produce five levels of line to line voltage and three levels of phase voltage. This NPC converter reduces harmonics in both voltage and current output [12 – 19].

Table 1 gives the switching states for phase; a similar switching sequence will be derived for other phases according to the phase angle displacement. Here, K_1 and K_2 are turned on giving $V_{dc}/2$ and K_3 and K_4 are turned on giving $-V_{dc}/2$ [11, 12].

Table 1
Switching states of three level NPC inverter.

States of switches				Voltages level
K_1	K_2	K_3	K_4	
on	on	off	off	$V_{dc}/2$
off	on	on	off	0
off	off	on	on	$V_{dc}/2$

7   PWM Strategy

A NPC inverter includes the DC power source for output of DC voltage having a neutral point. An NPC converts a DC voltage into an AC voltage in three phases PWM control. When a mode is selected, consider for a first and a second PWM mode by comparing the amplitude of voltage reference with a predefined value that is defined by a minimum pulse width, a first voltage reference means to add a predefined bias value at which a change to positive/negative within a fixed period to voltage references in respective phases in a first PWM mode, a

second voltage reference means to fix the voltage reference in one phase by a value with minimum pulse width when voltage reference in one phase is smaller than a described value that is defined by the minimum pulse width in a next PWM mode and correct voltage references of other two phases so as to make line voltage to a value corresponding to the voltage reference, and a modulation frequency varied over to lower PWM control modulation frequency in the first PWM mode and to suppress power loss caused by switching in the first PWM mode [18].

The Fig. 3 shows the modulation strategy for three-level NPC inverter. PWM strategy is applied for arms.

In Fig. 3, C_1 and C_2 are triangular carriers of three Arm (A, B, C), V_a represents the modulation wave of Arm A. The phase of C_1 is opposite with C_2.

When the value of V_a is higher than C_1, K_1 and K_2 are switched on. When the value of V_a is lower than C_2, K_3 and K_4 are switched on. In the other case, K_2 and K_3 are turned on, and the output level is 0. Similarly, C_1 and C_2 are triangular carriers of Arms B and C, V_b represents the modulation wave of Arm B and V_c represents the modulation wave of Arm C. the same principle applied for arm A is applied for two arms B and C [18].
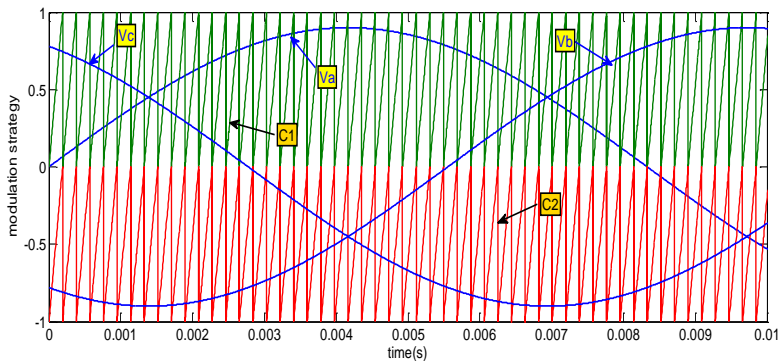
Fig. 3 – *Modulation strategy of three level NPC Inverter.*

8 LCL Filter

Excessive heating in the motor depends on the THD generated by the three-level NPC inverter. Harmonic distortion produces elastic deformation such as shaft deflection, parasitic torques, vibration noise, additional heating, and lower the efficiency of induction motors.

The harmonic current/voltage flowing in the induction motor's, causes additional heating effects on stator windings, in the conductors, and iron parts in the motor [20].

Negative-class harmonics cause additional losses by inducing high frequency currents and negative torques in machine rotors [16, 17].

Due to the pulsating voltage at the three-level NPC inverter output nodes, LCL filter placed between the inverter and the induction motor to attenuate the switching harmonics. The filter is usually composed of inductors and capacitors. With this filter, the switching frequency of the converter has to be high enough to reduce the harmonic distortions at the stator windings [20].

The LCL filter used to obtain a higher attenuation as well as cost savings, is also one of the advantages of the overall reduction of the weight and size of the components. The LCL filter is consisting of L_1, L_2, L_3 inductances at the NPC three level inverter- side, inductances L_4, L_5, L_6 at the induction motor side, and capacitances C_1, C_2, C_3 in-between, as it is shown in Fig. 4. LCL filters have been used in induction motor-connected inverters, because they minimize the amount of current and voltage distortion injected into the induction motor. The excellent performance can be obtained in the range of power levels up to hundreds of kW, with the use of small values of inductances and capacitances.

The parameters of used induction motor, NPC inverter and LCL filter are given in **Table 2.**

<div align="center">

Table 2

Parameters of system components.

</div>

Parameters of induction motor:
$P = 1.5[\text{kW}]$, $F = 50[\text{Hz}]$, $V = 220/380[\text{V}]$, $p = 2$ pole pairs, $L_r = 0.274[\text{mH}]$, $L_s = 0.274[\text{mH}]$, $R_s = 4.85[\Omega]$, $L_m = 0.258[\text{mH}]$, $J = 0.031[\text{Kg m}^2]$, $f = 0.0114[\text{Nms/rad}]$, $\omega_s = 2\pi50[\text{rad/s}]$
NPC inverter : $V_{dc} = 380[\text{V}]$
Parameters of LCL filter
$C_1 = C_r = C_3 = 0.5[\text{F}]$, $L_1 = L_r = L_3 = L_4 = L_5 = L_6 = 0.06[\text{mH}]$

9   NPC Three Level Inverter Fault Analysed

Inverter power switch faults are subdivided into short and open circuit [14].

Short circuits, in most cases, that can lead to brutal damages on the switch itself or even on the drive. These faults usually cause the tripping of fuses and, in intolerant structures (conservative design), the turn-on of spare power switches [13, 14].

Open-Switch Faults that have a less immediate negative effect. However, the cumulative effect may lead to non-reversible degradation [8, 9].

Open-Circuit Fault in K_1: To generate a positive switching state, K_1 and K_2 must be turned on, and positive currents will pass through these switching devices. While, when K_1 fault occurs, another current path is formed, from D_1 and K_1. Output current decreases to 0. When K_1 fault occurs, the switching positive state can't work as normal [8, 9].

The output voltage is equal to the reference value (200 V) and the output current reaches to 1.4 A in the full-load condition, and all capacitors have the same voltage value (100 V). The voltage of capacitors is equal to half of the DC-link voltage because of their serial connection.

The Fig. 4 shows the structure of the three-level inverter controlled by PWM, also observes the default application on the three switches K_1, K_7 and K_{10}, this figure shows the use of LCL filter which is used to filter the voltage output and output current of the three-level NPC inverter.
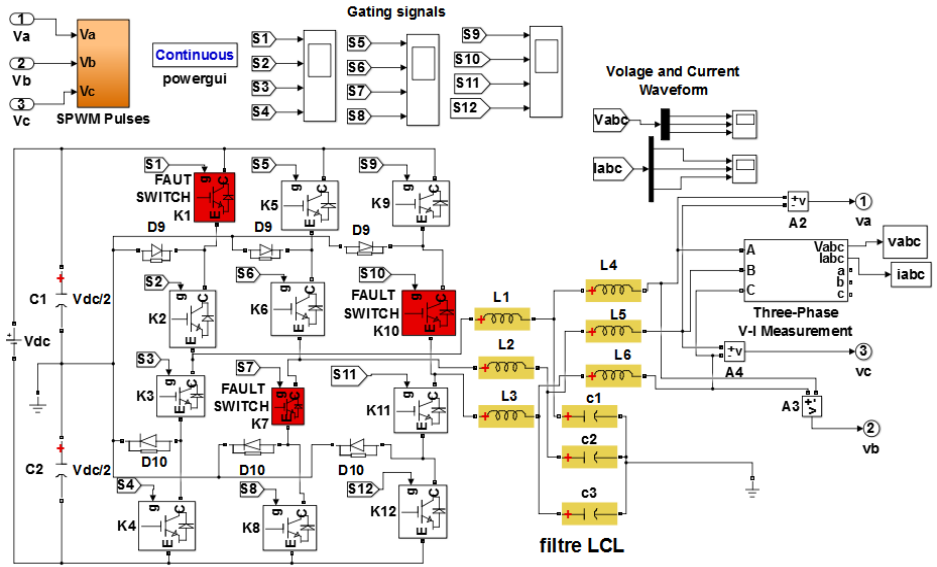
Fig. 4 – *Three level NPC inverter structure with K_1, K_7 and K_{10} switch fault.*

In Fig. 5 shown the three-phase voltage of phase A, and B, under K_1 and K_7 open-circuit fault, it can be seen that the amplitudes of three-phase voltage decreased. During open circuit faults of switches K_1, K_7 and K_{10}, the three-phase voltages are no longer symmetric, and changed most significantly. The phase voltage of phase A, B and C distorted because of the open-circuit fault.
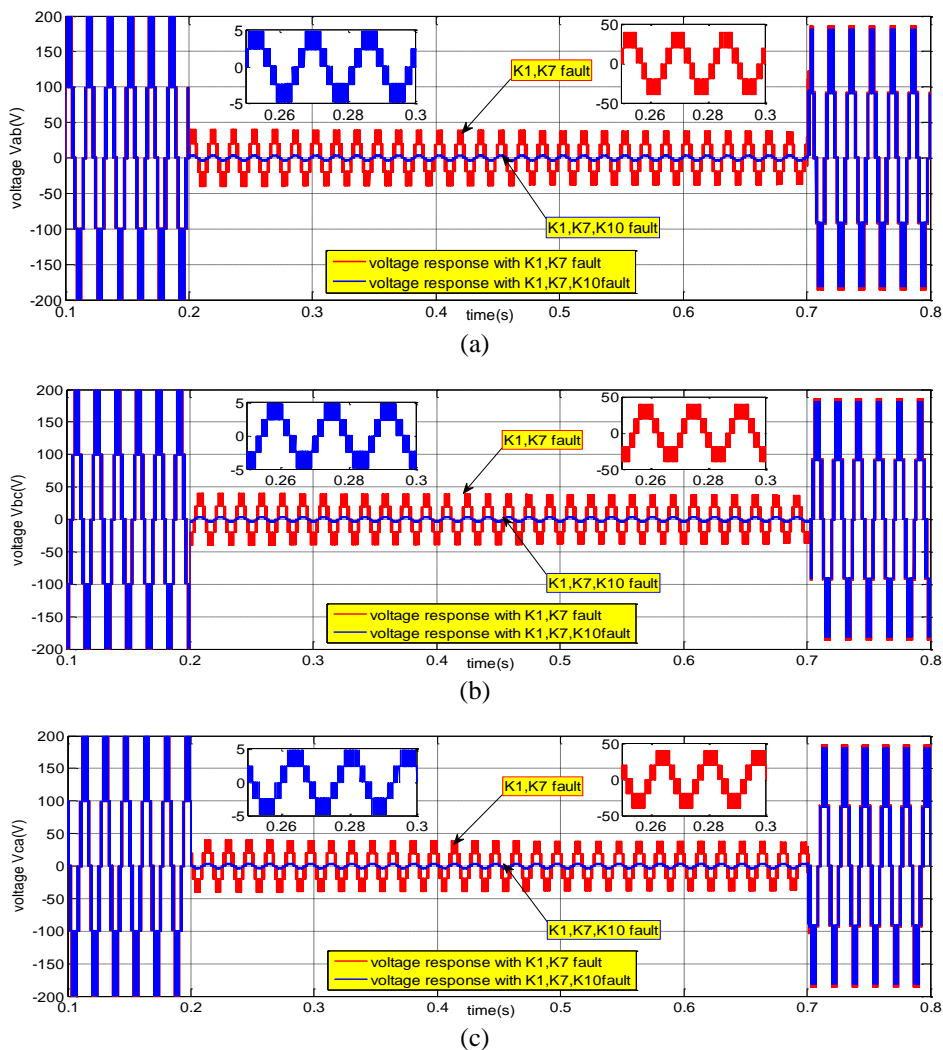
Fig. 5 – (a) *Output voltage* V_{ab} ; (b) *Output voltage* V_{bc} ; (c) *Output voltage* V_{ca} *with existence of switches* K_1, K_7 , *and* K_1, K_7, K_{10} *fault of three level NPC inverter.*

The three level NPC inverter outputs line-line voltages with three states. The system is operating normally before 0.2 s witch the output voltages equal to 200V. In the time interval [0.2, 0.7]s, two faults are applied, the first fault will be applied on two switches K_1, K_7 and the second will be on three switches K_1, K_7, K_{10}. When the switch fault K_1 and K_7 occurs in the time interval [0.2, 0.7]s, the output voltage of NPC three level inverters is distorted and the level of the output voltage is

reduced, which the output voltage equal 49.9 V. But during switches faults K_1, K_7 and K_{10}, we observed more reduction on output voltages which equal to 5 V.

From Fig. 6, it can be seen that when K_1 and K_7 come into open-circuit fault at the same time, the three-phase filtered output current is no longer symmetric, and the current of phase A, B and C changed the most obvious. The filtered output current which is equal to the reference current before the fault (1.4 A) but during the switch fault K_1, K_7 in the time interval [0.2, 0.7] s, the output filtering current decreases to 0.28 A, this decrease well notices on the current zooms.

In Fig. 7 it can be seen that when K_1, K_7 and K_{10} come into open-circuit fault at the same time, the phase filtered output current of phase A, B and C changed to 0 after the fault occurred. The filtered output current decreased to 0.032 A during the switch fault K_1, K_7 and K_{10} in the time interval [0.2, 0.7] s. This decrease of the current value is observed by their reduction, which is well noticed on the current zooms.

From Fig. 8, it can be seen that when K_1 and K_7 come into open-circuit fault at the same time, the amplitude of filtered output voltage phase A, B and C has also decreased. The filtered output voltage, which is equal to the reference voltage before the fault (200 V) but during the application of a switch fault K_1, K_7 notices a significant decrease in the output filtering voltage (49.9 V). This decrease is well noticed on the voltage zooms.

From Fig. 9 it can be seen that the amplitudes of the three-phase filtered output voltage have been decreased and changed after the fault occurred during the switch fault K_1, K_7 and K_{10}. The filtered output voltage decreased to 5 V during the switch fault K_1, K_7 and K_{10} in the interval time [0.2, 0.7] s. This decrease in the value of the voltage is observed by their reduction or cancellation, which is well noticed on the voltage zooms.
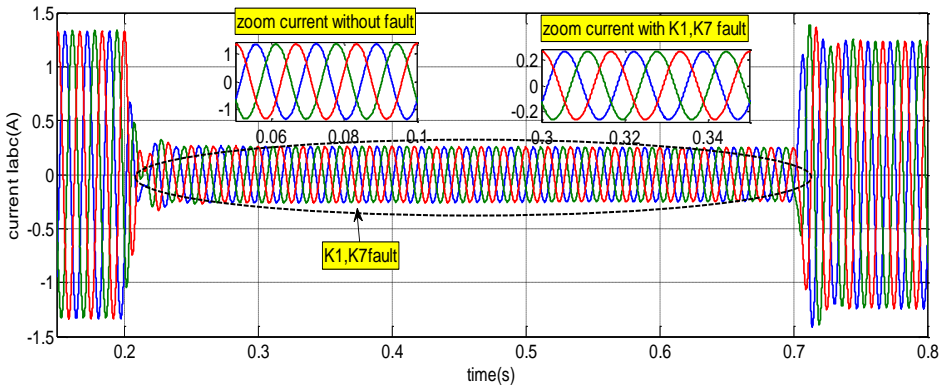
Fig. 6 – *Filtering current I_{abc} with existence of switches*
K_1, K_7 fault of three level NPC inverter.
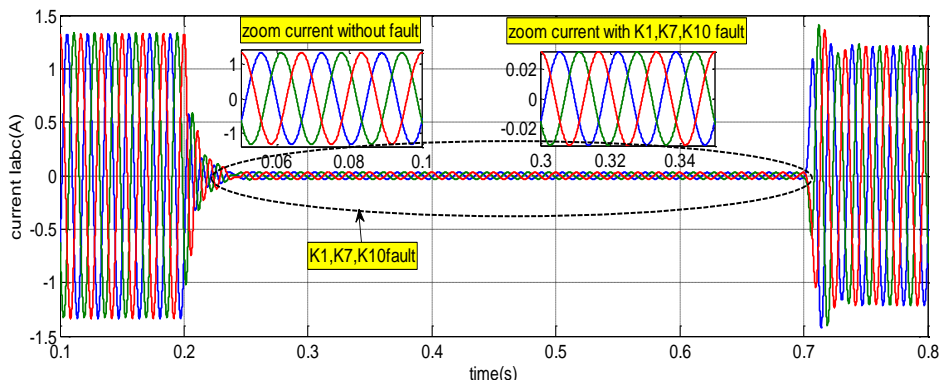
Fig. 7 – *Filtering current I_{abc} with existence of switches K_1, K_7, K_{10} fault of three level NPC inverter.*
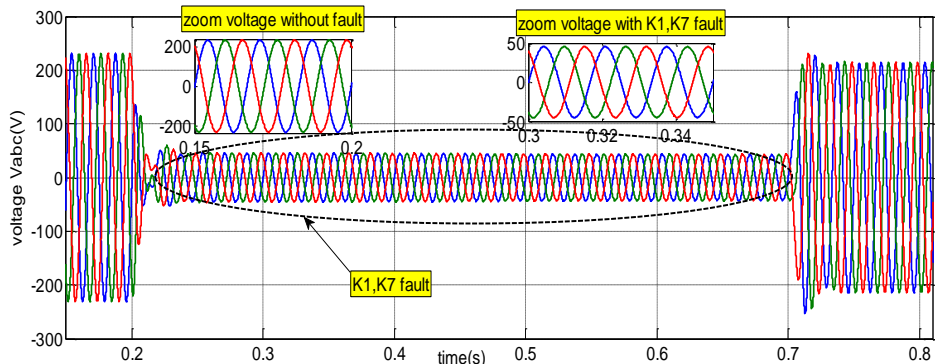
Fig. 8 – *Filtering output voltage V_{abc} with existence of switches K_1, K_7 fault of three level NPC inverter.*
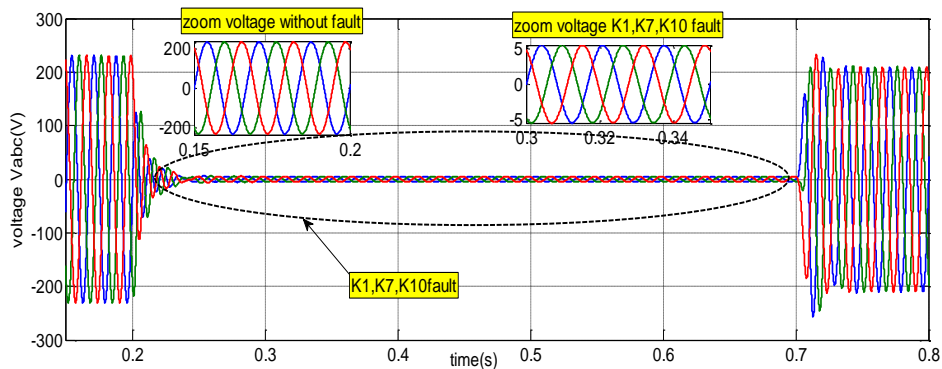
Fig. 9 – *Filtering output voltage V_{abc} with existence of switches K_1, K_7, K_{10} fault of three level NPC inverter.*

10 Simulation Results and Discussion

Inverter switching faults reduce the performance of the motor; in our study, we associate the induction motor with a three-level NPC inverter where we apply a fault in the switches to test the performance of input-output linearization command on the physical parameters of the induction motor, the simulation will be shown by the following results.

The Fig. 10 shows the simulation results for the input-output speed linearization control for induction motor associated with three-level NPC inverter.

The machine is applied with a load torque of 10 Nm in time 0.1 s; the direction of rotation of the machine is reversed from 157 rad/s to -157 rad/s in time 1.7 s. When the motor starts with reference speed 50 rad/s in the time interval [0.1, 0.7] s, it is found that the speed without applying the switch fault of three-level NPC inverter joins its reference. During rotation sense's reversing, the speed controller shows a similar behaviour to the start-up state by operating the system at the physical limit. The speed is shown good transient and steady state reference tracking dynamics.

The simulation results show that the speed input-output linearization control without switch fault application is robust to the variation of the reference speed, since the speed measured without fault tracks the reference speed at startup as well as the reversal of the direction of rotation, in a very satisfactory way. We can clearly see the dynamic insensibility of the proposed strategy for the low speed induction motor.

When applying the fault K_1, K_7, K_{10} a very significant decrease in the speed rate reaches up to -60 rad/s compared to K_1, K_7 fault in the time interval [0.2, 0.7]s in the three-level NPC inverter associated with the induction motor by the use of input-output linearization control, it is found that this type of defect causes a disturbed and unstable operation of the system due to the change of operation mode during the application of the defect. This decrease is clearly noticeable on the speed zooms.

In the Fig. 11 it can also be noticed that the torque rate also shows very strong ripples during the fault K_1, K_7, K_{10} compared to K_1, K_7 fault. This ripple can be seen well on the torque zooms.

Open-circuit IGBT failures are introduced by disabling the control signals of switches. It can be observed that the induction motor is in a stable steady-state condition with torque held at 10 Nm. During K_1, K_7 open circuit in two phases A and B we see a peak-to-peak ripple of 100 Nm but with the application of K_1, K_7 and K_{10} open circuit in three phases A, B and C we notice an increase in peak to 200 Nm, respectively. In the faulty state, the drive system loses control of the

induction motor and does not produce any torque when the switches are in open-circuit. Thus, the machine naturally decelerates to rest.
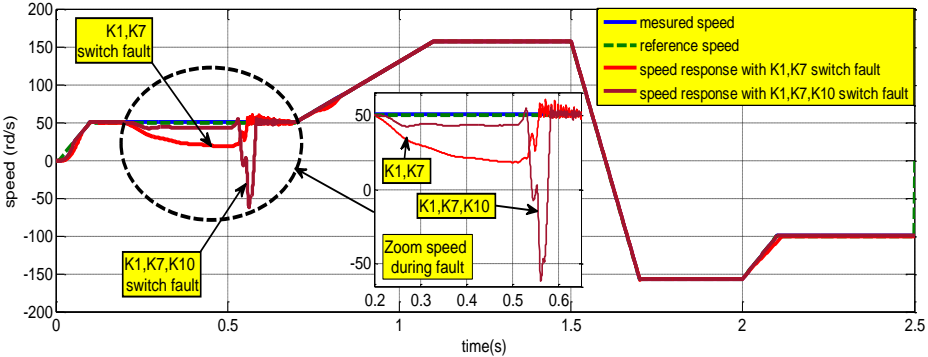
Fig. 10 – *Speed result of induction motor with input output linearization control and application switch fault in three-level NPC inverter.*

When the fault occurs in the three-level NPC inverter switches, the current has a sudden drop that has produced a drop on the response of the flux. The drops that occur in the currents and fluxes when the switch fault occurs, causing a sudden drop in the torque that allows it to take a maximum value in the negative direction.

The result is that the fault can damage other components and endanger the system operation in the presence of this type of inverter fault.
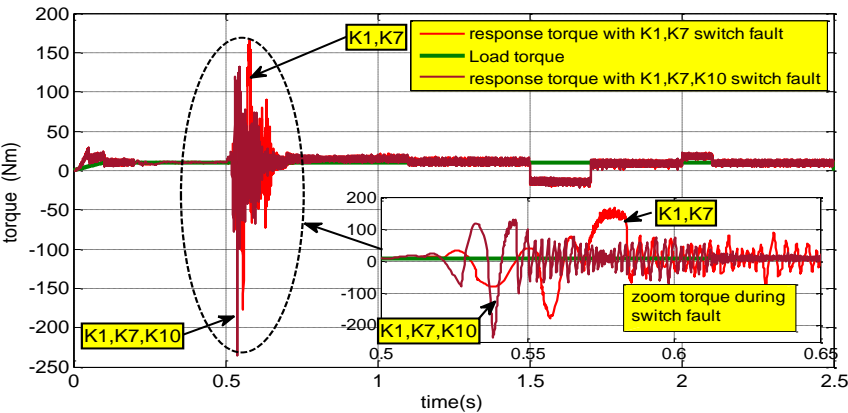
Fig. 11 – *Torque result of induction motor with input output linearization control and application switch fault in three level NPC inverter.*

The Fig. 12 shows that during the switches fault K_1, K_7, K_{10} compared to K_1, K_7 fault in the time interval [0.2, 0.7] s, we can see a strong increase that causes an imbalance in the flux response, where their amplitude reaches a very high value that leads to the degradation of the system and damage to the motor.

The Fig. 13 shows that during the switches fault K_1, K_7 and K_{10} compared to switches fault K_1, K_7 in the time interval [0.2, 0.7] s, we can see a strong increase that causes an imbalance in the rotor flux response $\varphi_{s\alpha}$ and $\varphi_{s\beta}$.
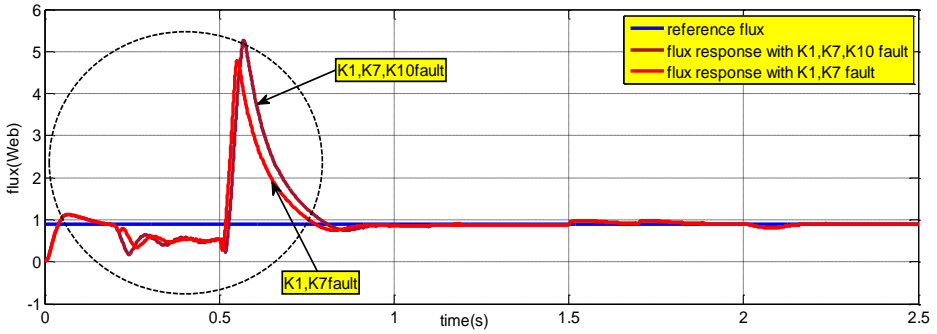
Fig. 12 – *Flux result of induction motor with input output linearization control and application switch fault in three level NPC inverter.*
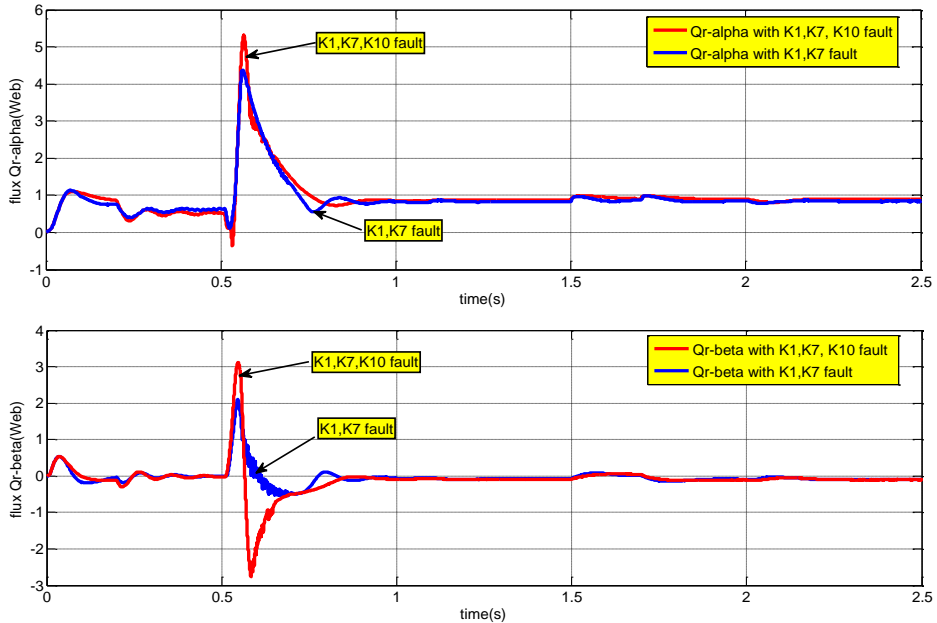
Fig. 13 – *Flux result of induction motor with input output linearization control and application switch in three level NPC inverter.*

When the switch faults occur in the three level NPC inverter, the stator current $I_{s\alpha}$ and $I_{s\beta}$ of the induction motor increases from its desired value, as shown in Fig. 14. That produced an increase of the flow.

The Fig. 14 shows that during the switches fault K_1, K_7 and K_{10} compared to switches fault K_1, K_7 in the time interval [0.2, 0.7] s, we can see a strong increase that produced imbalance in the stator current response $I_{s\alpha}$ and $I_{s\beta}$.

The Fig. 15 shows the dynamics of the static error speed with the existence of switch fault and without fault.
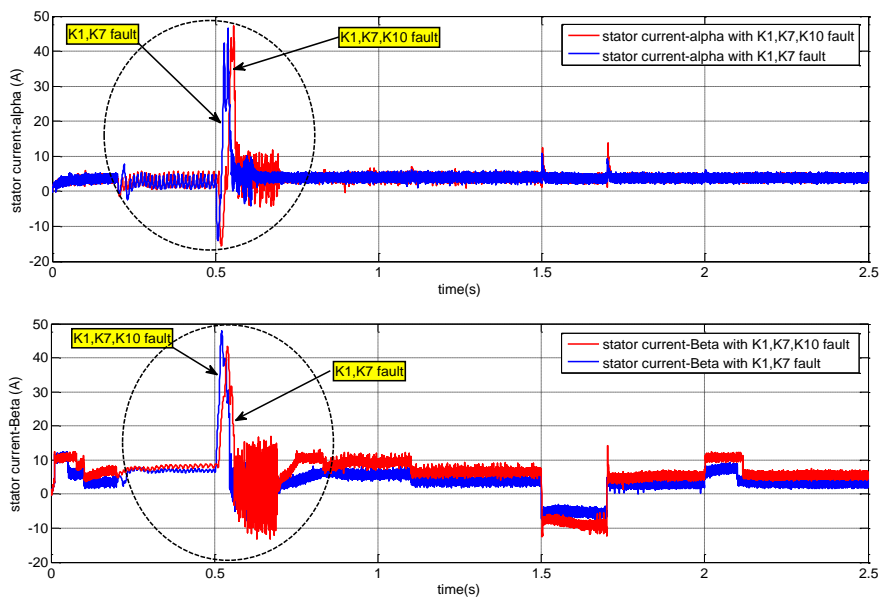
Fig. 14 – *Stator current result of induction motor with input output linearization control and application switch fault in three level NPC inverter.*
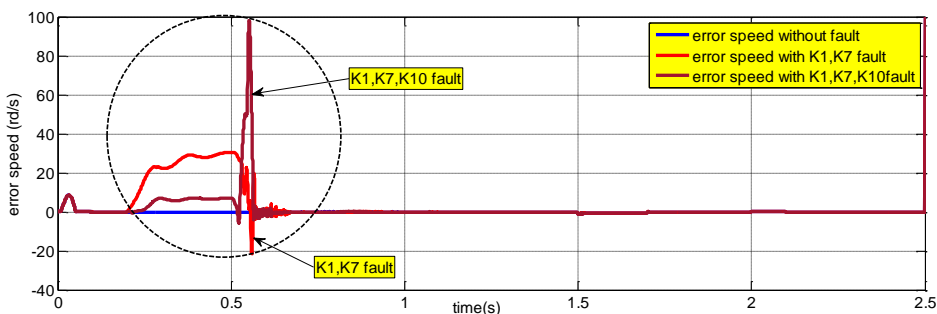
Fig. 15 – *Error speed result of induction motor with input output linearization control and application switch fault in three level NPC inverter.*

The tests performed to ensure the robustness of input-output linearization control against switch faults K_1, K_7 and K_1, K_7, K_{10} of the three level NPC inverter at high and low speeds. The static error speed response shows that the switch fault can cause degradation in the expected performance, mainly with respect to the reference speed tracking. The application of switch fault causes an important increase of static error speed; this increase is mainly allowed the speed to move away from its reference, which causes system instability.

11 Conclusion

In this paper, the input-output linearization approach is presented which is a way to algebraically transform nonlinearity, multivariable, complex and dynamic systems into linear ones, so that we can apply the linear control, this technique has attracted a lot of research in recent years. For this purpose, we have applied this proposed approach to derive the control of induction motor in this paper.

This control strategy ensures perfect linearization regardless of the profile trajectories physically imposed on the induction motor system. The decoupling between the two selected outputs (speed and flux) is then achieved, the proposed method confirm their effectiveness and superiority.

The three level NPC inverter presents a big interest in the field of the higher voltages and the high powers of the fact that they introduce less distortion and weak losses with relatively low switching frequency. Also, the use of three-level NPC inverter in combination with an induction motor with the use of the input-output linearization can reduce harmonics and have a higher output voltage level and improve the quality of the motor output signals.

To test the performance of the input-output linearization control, we apply faults on the three-level NPC inverter switches. Thus, the input-output linearization control enables us to have the influence of the existence of a fault on the physical parameters of the induction motor (speed, electromagnetic torque, and flux) which is on the decrease, increase, ripple and oscillation that disturb the different signals. The simulation study clearly indicates the superior performance of input-output linearization control. This superiority is observed in the responses that show the effect of fault.

12   References

[1]   S. Zaidi, F. Naceri, R. Abdessemed: Input-Output Linearization of an Induction Motor Using MRAS Observer, International Journal of Advanced Science and Technology, Vol. 68, July 2014, pp. 49 – 56.

[2]   O. Zaghib, A. Allag, M. Allag, B. Hamidani: Input-Output Linearization Control based on a Newly Extended MVT Observer Design: An Induction Machine Application, Journal of Electrical Engineering, Vol. 20, No. 5, December 2020, pp. 1 – 7.

[3]   A. Oukaci, R. Toufouti, D. Dib, L. Atarsia: Comparison Performance Between Sliding Mode Control and Nonlinear Control, Application to Induction Motor, Electrical Engineering, Vol. 99, No. 1, March 2017, pp. 33 – 45.

[4]   A. Accetta, M. Cirrincione, F. D'Ippolito, M. Pucci, A. Sferlazza: Input-Output Feedback Linearization Control of a Linear Induction Motor Taking into Consideration its Dynamic End-Effects and Iron Losses, Proceedings of the IEEE Energy Conversion Congress and Exposition (ECCE), Detroit, USA, October 2020, pp. 2419 – 2424.

[5]   F. Alonge, M. Cirrincione, M. Pucci, A. Sferlazza: Input-Output Feedback Linearization Control with On-Line MRAS-Based Inductor Resistance Estimation of Linear Induction Motors Including the Dynamic End Effects, IEEE Transactions on Industry Applications, Vol. 52, No. 1, January 2016, pp. 254 – 266.

[6]   F. Berrezzek, W. Bourbia, B. Bensaker: Nonlinear Control of Induction Motor: A Combination of Nonlinear Observer Design and Input-Output Linearization Technique, Proceedings of the 4th International Conference of Electrical Engineering, Algiers, Algeria, May 2012, pp. 467 – 472.

[7]   B. Kothapalli, R. Boini, M. Sai Kumar, A. Rajamallaiah: Multilevel Topology in Three-Level Inverter Fed Induction Motor Drive, International Journal of Advance Science and Technology, Vol. 29, No. 10s, October 2020, pp. 8846 – 8853.

[8]   E. Parimalasundar, N. S. Vanitha: Identification of Open-Switch and Short-Switch Failure of Multilevel Inverters Through DWT and ANN Approach Using LabVIEW, Journal Electrical Engineering and Technology, Vol. 10, No. 6, November 2015, pp. 2277 – 2287.

[9]   M. Lin, Y.- H. Li, L. Qu, Ch. Wu, G.- Q. Yuan: Fault Detection of a Proposed Three-Level Inverter based on a Weighted Kernel Principal Component Analysis, Journal of Power Electronics, Vol. 16, No. 1, January 2016, pp. 182 – 189.

[10] A. Yahiaoui, K. Iffouzar, K. Himour, K. Ghedamsi: Comparison of Different Multilevel Voltage Source Inverter Topologies on Induction Motor Energy Quality, European Journal of Electrical Engineering, Vol. 21, No. 4, August 2019, pp. 367 – 372.

[11] A. Rasulkhani, A. Taheri: A New Multilevel Inverter Topology with Component Count Redaction, International Journal of Industrial Electronics Control and Optimization, Vol. 2, No. 4, October 2019, pp. 355 – 364.

[12] W. Yuan, T. Wang, D. Diallo, C. Delpha: A Fault Diagnosis Strategy based on Multilevel Classification for a Cascaded Photovoltaic Grid-Connected Inverter, Electronics, Vol. 9, No. 3, March 2020, pp. 429.

[13] S. Cheng, J. Zhao, C. Chen, K. Li, X. Wu, T. Yu, Y. Yu: An Open Circuit fault- Diagnosis Method for Inverters Based on Phase Current: Transportation Safety and Environment, Vol. 2, No. 2, June 2020, pp. 148 – 160.

[14] S. S. Moosavi, A. Kazemi, H. Akbari: A Comparison of Various Open-Circuit Fault Detection Methods in the IGBT-Based DC/AC Inverter Used in Electrical Vehicle, Engineering Failure Analysis, Vol. 96, February 2019, pp. 223 – 235.

[15] W. Ghozlane, J. Knani: NonLinear Control via Input-Output Feedback Linearization of a Robot Manipulator, Advances in Science, Technology and Engineering Systems Journal, Vol. 3, No.5, October 2018, pp. 374 – 381.

[16] V. Meenakshi, S. Paramasivam: Design of LCL Filter in Front End Converters Suitable for Grid Connected Wind Electric Generators, Journal of Scientific and Industrial Research, Vol. 78, December 2019, pp. 896 – 899.

[17] M. Azab: Multi-Objective Design Approach of Passive Filters for Single-Phase Distributed Energy Grid Integration Systems Using Particle Swarm Optimization, Energy Reports, Vol. 6, November 2020, pp. 157 – 172.

[18] A. A. Kadum: PWM Control Techniques for Three Phase Three Level Inverter Drives, TELKOMNIKA (Telecommunication, Computing, Electronics and Control), Vol. 18, No. 1, February 2020, pp. 519 – 529.

[19] R. Palanisamy, K. Vijayakumar, K. Selvakumar, D. Karthikeyan, G. Santhoshkumar: Implementation of 5 Phase 3 Level NPC Inverter Using Space Vector Modulation, Indian Journal of Science and Technology, Vol. 9, No. 42, November 2016, pp. 1 – 6.

[20] S. Lim, J. Choi: LCL Filter Design for Grid Connected NPC Type Three-Level Inverter, International Journal of Renewable Energy Research, Vol. 5, No. 1, March 2015, pp. 45 – 53.

[21] Y. Fetene, D. Shibeshi: Fractional Order Sliding Mode Speed Control of Feedback Linearized Induction Motor, Power Electronics and Drives, Vol. 5, No. 1, January 2020, pp. 109 – 122.